PHYSICAL REVIEW D **76,** 054504 (2007)

Confining properties of QCD at finite temperature and density

Simone Conradi, Alessio D'Alessandro, and Massimo D'Elia

Dipartimento di Fisica dell'Università di Genova and INFN, Sezione di Genova, Via Dodecaneso 33, I-16146 Genova, Italy

(Received 12 June 2007; published 17 September 2007)

A disorder parameter detecting dual superconductivity of the vacuum is used as a probe to characterize the confining properties of the phase diagram of two-color QCD at finite temperature and density. We obtain evidence for the disappearing of dual superconductivity (deconfinement) induced by a finite density of baryonic matter, as well as for a coincidence of this phenomenon with the restoration of chiral symmetry both at zero and finite density. The saturation transition induced by Pauli blocking is studied as well, and a general warning is given about the possible effects that this unphysical transition could have on the study of the QCD phase diagram at strong values of the gauge coupling.

DOI: 10.1103/PhysRevD.76.054504 PACS numbers: 11.15.Ha, 12.38.Aw, 12.38.Gc

I. INTRODUCTION

Color confinement emerges as an absolute property of strongly interacting matter from experimental facts, but is not yet fully understood starting from the QCD first principles. Lattice QCD simulations, however, have given some evidence about confinement and have even predicted the presence of a finite temperature transition to a deconfined state of matter, which is currently under investigation in heavy ion collision experiments. Deconfinement, as seen by lattice simulations, appears to take place at the same temperature where other important physical phenomena happen, like for instance the restoration of chiral symmetry.

In the present study we address the question regarding the fate of confining properties in the presence of a finite density of baryonic matter: that is important in order to understand the structure of the QCD phase diagram both in the region of low densities and high temperatures, which is relevant for heavy ion experiments, and in the region of low temperatures and high densities, where the study of confining properties could help characterize the nature of matter in compact astrophysical objects. In particular we are interested in understanding how deconfinement induced by a critical density of baryonic matter compares to what happens at zero density, and how it is related to other possible transitions in the QCD phase diagram. Various possibilities are open in principle, like for instance a noncoincidence of the deconfinement transition with the restoration of chiral symmetry (see Ref. [1] for a recent discussion about this issue).

The topic has been already studied in previous literature. In particular, results about deconfinement at high densities and low temperatures have been obtained in Ref. [2], while the relation between deconfinement and the chiral transition has been investigated in Refs. [3,4]. However, previous studies have been based on the study of the expectation value of the Polyakov loop as a probe for the deconfinement transition: while that can indeed be used as an order parameter for confinement in the pure gauge theory, being related to the spontaneous breaking of the center symmetry, the same is not true in the theory with dynamical fermions, where center symmetry is explicitly broken. For that reason in the present study we look for different order parameters which are constructed in the framework of specific mechanisms of color confinement and which may be valid also in the full QCD theory.

One appealing mechanism, among others, is that based on dual superconductivity of the QCD vacuum, which relates confinement to the breaking of an Abelian dual symmetry induced by the condensation of magnetic monopoles [5–7]. The possibility to define disorder parameters in this scenario has been studied since a long time; one parameter has been developed by the Pisa group [8,9] and consists of the expectation value of an operator which creates a magnetic monopole, $\langle \mathcal{M} \rangle$[1]: that has been shown to be a good parameter for color confinement both in pure Yang-Mills theories [10,11] and in full QCD [12,13]; similar parameters have been developed elsewhere [14–16].

Our plan is to use $\langle \mathcal{M} \rangle$ as a parameter for characterizing the confining properties of the various phases in the QCD phase diagram. Since numerical studies of QCD at finite density are notoriously difficult because of the sign problem, which makes usual importance sampling simulations unfeasible, in the present study we restrict ourselves to the theory with two colors, where that problem is absent. In principle no significant differences are expected for the confining properties of the theory when going from $N_c = 2$ to $N_c = 3$, where N_c is the number of colors: for that reason we believe that our study could be relevant also for real QCD. Of course this is only partially true regarding the relation between deconfinement and chiral symmetry restoration, since more significant differences are expected for the latter when going from $N_c = 2$ to $N_c = 3$. In the low temperature region of the $N_c = 2$ theory, in particular, the chiral condensate is expected to disappear at the onset

[1]We change the usual notation for the disorder parameter, $\langle \mu \rangle$, in order to avoid confusion with the notation for the chemical potential.

of the superfluid phase related to diquark condensation, which moves towards lower values of the chemical potential as the quark masses are lowered.

In Sec. II we recall the general properties of lattice QCD at finite baryon density as well as the specific features of the two-color model. In Sec. III we review the definition of the disorder parameter $\langle \mathcal{M} \rangle$ and develop our strategy to study its properties at finite density. In Sec. IV we present our numerical results: in particular, in Sec. IV A we present a study of the disorder parameter at zero density; results at nonzero baryon density are given in Sec. IV B; a determination of the chiral transition line and its comparison with the deconfinement transition line are presented in Sec. IV C. In Sec. IV D the disorder parameter $\langle \mathcal{M} \rangle$ and other observables are used to study the nature of the unphysical transition to the saturation regime taking place at high values of the chemical potential, and the possible influence of saturation on the physical transition is discussed. In Sec. IV E we discuss the relevance of our results for the low temperature region of the phase diagram. Finally, in Sec. V, we draw our conclusions. A partial account of our results has been presented in Ref. [17].

II. QCD AT FINITE DENSITY AND THE TWO-COLOR MODEL

We will consider a discretized lattice action for two-color QCD at finite chemical potential defined as follows:

$$S = S_G + \sum_{i,j} \bar{\psi}_i M[U]_{i,j} \psi_i, \tag{1}$$

where S_G is the pure gauge Wilson action,

$$S_G = \beta \sum_{\square} (1 - \frac{1}{2} \mathrm{Tr} \square), \tag{2}$$

the sum being over all plaquettes, while the fermion matrix is defined, in the case of standard staggered fermions, as

$$M_{i,j} = am\delta_{i,j} + \frac{1}{2} \sum_{\nu=1}^{3} \eta_{i,\nu} (U_{i,\nu} \delta_{i,j-\hat{\nu}} - U^{\dagger}_{i-\hat{\nu},\nu} \delta_{i,j+\hat{\nu}}) + \eta_{i,4} (e^{a\mu} U_{i,4} \delta_{i,j-\hat{4}} - e^{-a\mu} U^{\dagger}_{i-\hat{4},4} \delta_{i,j+\hat{4}}). \tag{3}$$

Here i and j refer to lattice sites, $\hat{\nu}$ is a unit vector on the lattice, $\eta_{i,\nu}$ are staggered phases, and U are gauge link variables; $a\mu$ and am are, respectively, the chemical potential and the quark mass in lattice units. The grand-canonical partition function can be written, after integrating out fermions, as

$$Z = \int \mathcal{D}U e^{-S_G[U]} \det M[U]. \tag{4}$$

In ordinary QCD the fermion determinant is complex for generic values of the chemical potential, thus hindering numerical Monte Carlo simulations. Various possibilities have been explored to circumvent the problem, like for instance reweighting techniques [18,19], the use of an imaginary chemical potential either for analytic continuation [3,20–25] or for reconstructing the canonical partition function [26–28], Taylor expansion techniques [29,30], and nonrelativistic expansions [31–33].

The problem is absent in QCD with two colors, since the gauge group is real: indeed the fermion determinant, being expressible like any other gauge invariant observable in terms of traces over closed loops, is real as well, and numerical simulations are feasible. For this reason two-color QCD has been widely studied in the past as a laboratory for real QCD at finite density [2,4,34–40]. Despite some peculiar features of the model, like the fact that baryons and mesons are degenerate, one still expects to learn relevant information about specific questions, like for instance the fate of topology [4] or confinement at finite density.

III. THE DISORDER PARAMETER $\langle \mathcal{M} \rangle$

The magnetically charged operator $\mathcal{M}(\vec{x}, t)$, whose expectation value detects dual superconductivity, is defined in the continuum as the operator which creates a magnetic monopole in $\vec{x}$, t by shifting the quantum field by the classical vector potential of a monopole, $\vec{b}_{\perp}$, and can be written (see Ref. [9] for details) as

$$\mathcal{M}(\vec{x}, t) = \exp\left[\frac{i}{e} \int \mathrm{d}^3 y \vec{E}_{\perp}(\vec{y}, t) \vec{b}_{\perp}(\vec{y} - \vec{x}) \right], \tag{5}$$

with the electric field $\vec{E}_{\perp}(\vec{y}, t)$ being the momentum conjugate to the quantum vector potential. $\vec{E}_{\perp}$ is defined after Abelian projection ($\sigma_3/2$ is the only possible diagonal generator in the case of $SU(2)$) in a given gauge. In the present paper we work in the so-called random Abelian projection defined in Ref. [11], where it has been shown that numerical results are independent of the particular gauge chosen.

The expectation value of the operator $\mathcal{M}$, when discretized on the lattice, can be expressed as the ratio of two different partition functions,

$$\langle \mathcal{M} \rangle = \tilde{Z}/Z, \tag{6}$$

where Z is the usual QCD partition function, while $\tilde{Z}$ is obtained from Z by a change in the pure gauge action $S_G \to \tilde{S}_G$, consisting in the addition of the monopole field to the temporal plaquettes at a given timeslice where the monopole is created. It has been shown in Ref. [16] that $\langle \mathcal{M} \rangle$ is equivalent to different definitions like that adopted in Ref. [16], up to $O(a^2)$. Differences are therefore present at finite lattice spacing, which however disappear in the continuum limit and are expected to be irrelevant for investigating large scale properties such as those related to phase transitions.

Being expressed as the ratio of two different partition functions, the numerical study of $\langle \mathcal{M} \rangle$ is a highly non-

trivial task, since $\mathcal{M}$ gets significant contributions only on those configurations having very small statistical weight. While numerical methods have been recently developed which permit a direct determination of $\langle\mathcal{M}\rangle$ [41], we shall not use them in the present study since they involve the combination of several different Monte Carlo simulations, a task which in presence of dynamical fermions could be unpractical. We will instead study, as usual, susceptibilities of the disorder parameter, from which the behavior of $\langle\mathcal{M}\rangle$ at the phase transition can be inferred.

For instance, being interested in $\langle\mathcal{M}\rangle$ as a function of β, as for the $\mu = 0$ phase transition, one usually measures [8–10]

$$\rho = \frac{\partial}{\partial\beta}\ln\langle\mathcal{M}\rangle = \frac{\partial}{\partial\beta}\ln\tilde{Z} - \frac{\partial}{\partial\beta}\ln Z = \langle S\rangle_S - \langle\tilde{S}\rangle_{\tilde{S}}, \quad (7)$$

where the subscript indicates the pure gauge action used for Monte Carlo sampling. The disorder parameter can be reconstructed from the susceptibility ρ, exploiting the fact that one has exactly $\langle\mathcal{M}\rangle = 1$ at $\beta = 0$

$$\langle\mathcal{M}\rangle(\beta) = \exp\left(\int_0^\beta \rho(\beta')\mathrm{d}\beta'\right). \quad (8)$$

In particular $\rho \simeq 0$ in the confined phase means $\langle\mathcal{M}\rangle \neq 0$, a sharp negative peak of ρ at the phase transition implies a sudden drop of $\langle\mathcal{M}\rangle$, and ρ diverging in the thermodynamical limit in the deconfined phase means that $\langle\mathcal{M}\rangle$ is exactly zero beyond the phase transition.

Studying $\langle\mathcal{M}\rangle$ as a function of β is what is usually done if one is interested in the fate of dual superconductivity as the temperature is increased. Indeed, in the Euclidean path integral formulation of QCD, the physical temperature is related to the inverse temporal extension, $T = 1/(L_t a)$, where a is the lattice spacing which for an asymptotically free field theory is a decreasing function of the inverse gauge coupling β. For that reason the inverse coupling β is usually adopted in place of T when studying the QCD phase diagram, the latter being an increasing function of the former.

At finite temperature and density we are interested in studying the behavior of $\langle\mathcal{M}\rangle$ in the two parameter space $(\beta, \hat{\mu})$, where $\hat{\mu} \equiv a\mu$ is the chemical potential in lattice units. For that reason we introduce the new susceptibility

$$\rho_D \equiv \frac{\partial}{\partial\hat{\mu}}\ln\langle\mathcal{M}\rangle = \frac{\partial\ln\tilde{Z}}{\partial\hat{\mu}} - \frac{\partial\ln Z}{\partial\hat{\mu}} = \langle N_q\rangle_{\tilde{S}} - \langle N_q\rangle_S, \quad (9)$$

where N_q is the quark number operator, i.e., according to the definition of Z given in Eq. (4),

$$\langle N_q\rangle = \left\langle \mathrm{Tr}\left(\frac{\partial M}{\partial\hat{\mu}}\cdot M^{-1}\right)\right\rangle \quad (10)$$

[an additional factor 2 is actually needed for the case studied in the present paper, which deals with 8 staggered flavors, see Eq. (12)]. The dependence of $\langle\mathcal{M}\rangle$ on the chemical potential μ can then be reconstructed as follows:

$$\langle\mathcal{M}\rangle(\beta,\hat{\mu}) = \langle\mathcal{M}\rangle(\beta,0)\exp\left(\int_0^{\hat{\mu}}\rho_D(\hat{\mu}')\mathrm{d}\hat{\mu}'\right),$$

so that, if the starting point at $\hat{\mu} = 0$ is in the confined phase ($\langle\mathcal{M}\rangle(\beta,0) \neq 0$), the behavior expected for $\rho_D(\hat{\mu})$ in correspondence of a possible finite density deconfinement transition will be the same shown by ρ across the finite temperature transition.

Assuming the presence of a (pseudo)critical line in the $T - \mu$ plane where the disorder parameter drops to zero and dual superconductivity disappears, the two susceptibilities ρ and ρ_D can be used not only to locate the position of the line, but also to compute its slope, thus providing a more comprehensive information about the QCD phase diagram. Indeed, it is quite natural to assume that the gradient of the disorder parameter,

$$\vec{\nabla}\langle\mathcal{M}\rangle = \left(\frac{\partial\langle\mathcal{M}\rangle}{\partial\beta}, \frac{\partial\langle\mathcal{M}\rangle}{\partial\hat{\mu}}\right) = (\rho,\rho_D)\langle\mathcal{M}\rangle, \quad (11)$$

be orthogonal, in the $\beta - \hat{\mu}$ plane, to the critical line, whose slope is then equal to $-\rho_D/\rho$. In the following we shall directly check this property on our numerical data and also make use of it to obtain testable predictions.

IV. NUMERICAL RESULTS

In order to perform numerical simulations we have adopted the usual hybrid Monte Carlo algorithm. The partition function in Eq. (4) can be rewritten, introducing pseudofermionic fields Φ, as

$$\begin{aligned} Z &= \int \mathcal{D}U\mathcal{D}\Phi\mathcal{D}\Phi^* e^{-S_g[U]-\Phi^*(M^\dagger M)^{-1}\Phi} \\ &= \int \mathcal{D}U e^{-S_g[U]}(\det M[U])^2. \end{aligned} \quad (12)$$

In the presence of a real chemical potential the usual even-odd factorization trick for reducing the number of flavors cannot be performed, so that Eq. (12) actually describes a theory with 8 (degenerate in the continuum limit) flavors. The standard exact ϕ algorithm described in Ref. [42] has been used.

We have performed simulations on lattices $L_s^3 \times L_t$ with $L_t = 6$ and different values of the spatial size ranging from $L_s = 8$ to $L_s = 16$. The bare quark mass has been fixed to $am = 0.07$. Two different simulations have been necessary, for each parameter set, using the two different pure gauge actions S and $\tilde{S}$ in order to reconstruct the susceptibilities ρ and ρ_D [see Eqs. (7) and (9)]. The typical run length has ranged from 2000 to 5000 molecular dynamics units. In order to maintain a reasonable acceptance the integration step δt has been varied from 0.01 to 0.002 depending on the values of β and μ. In particular quite small integration steps have been necessary for $a\mu > 0.3$ at the lowest value of β explored ($\beta = 1.45$), where the

appearance of small eigenvalues of the fermionic matrix makes the molecular dynamics less stable. The same phenomenon has influenced the noisy determination of fermionic observables, like the quark number entering the determination of ρ_D. $O(10)$ random vectors have been typically used for each gauge configuration in order to reduce the noise.

Simulations on the smallest lattice ($L_s = 8$) have been performed on a PC farm, making use of a numerical code obtained by adapting the publicly available MILC code for two colors and for the inclusion of a finite chemical potential. Simulations on larger lattices have been performed instead on the INFN apeNEXT facility in Rome.

The observables we look at are, apart from the susceptibilities of the disorder operator introduced in Sec. III, the average Polyakov loop, the average plaquette, and the chiral condensate:

$$\langle L \rangle \equiv \frac{1}{L_s^3} \sum_n \frac{1}{N_c} \langle \mathrm{Tr} \mathbf{L}(n) \rangle, \tag{13}$$

$$\langle P \rangle \equiv \frac{1}{6 L_t L_s^3} \sum_{n,\mu<\nu} \frac{1}{N_c} \langle \mathrm{Tr} \Pi_{\mu\nu}(n) \rangle, \tag{14}$$

$$\langle \bar{\psi}\psi \rangle \equiv \frac{1}{L_t L_s^3} \langle \mathrm{Tr} M^{-1} \rangle, \tag{15}$$

as well as their susceptibilities

$$\chi_c \equiv L_s^3 L_t \langle (\bar{\psi}\psi - \langle \bar{\psi}\psi \rangle)^2 \rangle, \tag{16}$$

$$\chi_L \equiv L_s^3 \langle (L - \langle L \rangle)^2 \rangle, \tag{17}$$

$$\chi_P \equiv L_s^3 L_t \langle (P - \langle P \rangle)^2 \rangle. \tag{18}$$

Notice that in the case of the chiral susceptibility we have explicitly considered only the disconnected contribution.

A. The deconfining transition at zero chemical potential

It is a well-known fact that in ordinary full QCD at zero baryon density, chiral symmetry restoration takes place at the same critical temperature as deconfinement, with the latter identified with the disappearance of dual superconductivity [12,13]. We will check again this fact for the theory with two colors, since this will be an important reference information for our following analysis at finite density.

We show in Fig. 1 the peaks of the three susceptibilities χ_c, χ_L, and χ_P defined above, obtained on a $16^3 \times 6$ lattice, together with curves corresponding to best fits to the location of their peaks. Our estimate for the location of the transition, obtained through a fit to the chiral susceptibility, is $\beta_c = 1.582(2)$, to be compared to those obtained by fitting the Polyakov loop susceptibility ($\beta_L = 1.587(4)$) and the plaquette susceptibility ($\beta_P = 1.575(5)$). A clear drop of the chiral condensate and a rise of the Polyakov loop are also observed at β_c, as shown in Fig. 2. The dependence of β_c on the spatial size is not significant, as can be appreciated from Table I, where we report a summary of the pseudocritical couplings (and chemical potentials) obtained from our simulations.

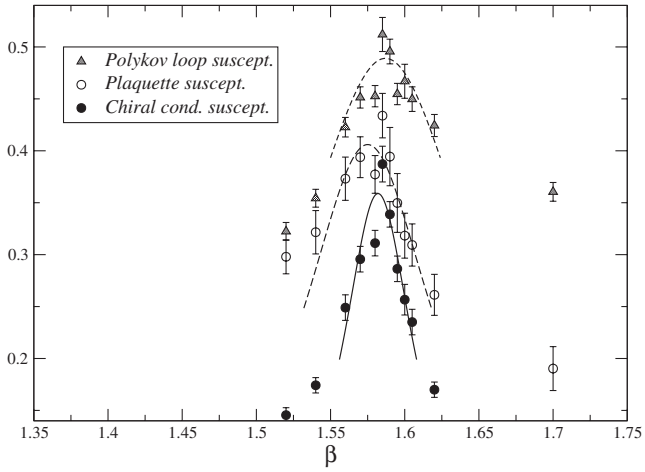

FIG. 1. Plaquette, Polyakov, and chiral susceptibilities on the $16^3 \times 6$ lattice at $\hat{\mu} = 0$. The chiral and the plaquette susceptibility have been, respectively, divided by a factor 10 and multiplied by a factor 4 in order to fit in the figure. Curves corresponding to best fits of the peak positions are superposed to the numerical data.

Let us now consider the fate of dual superconductivity. In Fig. 3 we show the behavior of the susceptibility ρ as a function of β for three different lattice sizes. A clear peak can be appreciated, which deepens when increasing the lattice size and whose location is clearly coincident with

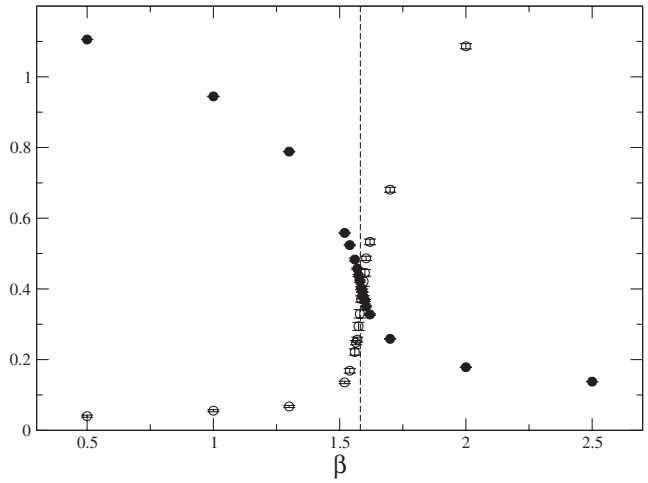

FIG. 2. Chiral condensate and average Polyakov loop as a function of β measured on a $16^3 \times 6$ lattice at $\hat{\mu} = 0$. The vertical line indicates the pseudocritical coupling β_c as determined from a best fit to the peak of the chiral susceptibility. The Polyakov loop has been multiplied by a factor of 15 to better fit in the figure.

TABLE I. Collection of pseudocritical couplings as determined from our numerical data. Physical critical couplings have been determined through the chiral susceptibility, while the unphysical saturation transitions have been located by means of the plaquette susceptibility.

L_s	β_c	μ_c
$8^3 \times 6$	1.584(2)	0
$12^3 \times 6$	1.587(2)	0
$16^3 \times 6$	1.582(2)	0
$16^3 \times 6$	1.568(2)	0.15
$8^3 \times 6$	1.55	0.222(10)
$16^3 \times 6$	1.55	0.215(10)
$8^3 \times 6$	1.5	0.325(10)
$12^3 \times 6$	1.5	0.349(15)
$16^3 \times 6$	1.5	0.342(10)
	β_{Sc}	μ_{Sc}
$8^3 \times 6$	1.55	0.678(20)
$8^3 \times 6$	1.675	0.793(10)
$16^3 \times 6$	1.675	0.789(22)

that of the chiral transition. Moreover it is also apparent from the figure that ρ is practically independent of the lattice size in the strong coupling region, confirming that $\langle \mathcal{M} \rangle \neq 0$ in the thermodynamical limit in that phase, while ρ strongly depends on L_s, and, in particular, is linear with it, as shown in Fig. 4, in the weak coupling region, showing that $\langle \mathcal{M} \rangle$ is exactly equal to zero in the thermodynamical limit beyond the transition (magnetic charge superselection [43]). Therefore β_c seems to separate two phases characterized by a different realization of the $U(1)$ magnetic symmetry.

To better appreciate the coincidence of the chiral transition with the disappearance of dual superconductivity, we have tried a finite size scaling (FSS) analysis of the critical behavior of $\langle \mathcal{M} \rangle$ around the transition temperature. We can

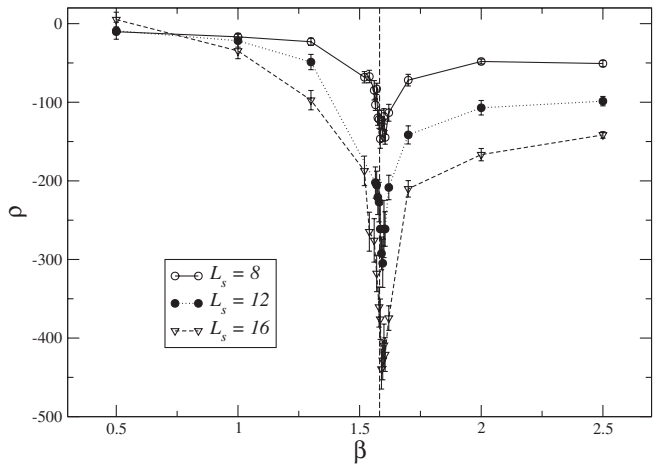

FIG. 3. ρ parameter as a function of β on various lattice sizes. The vertical line corresponds again to the location of the chiral transition.

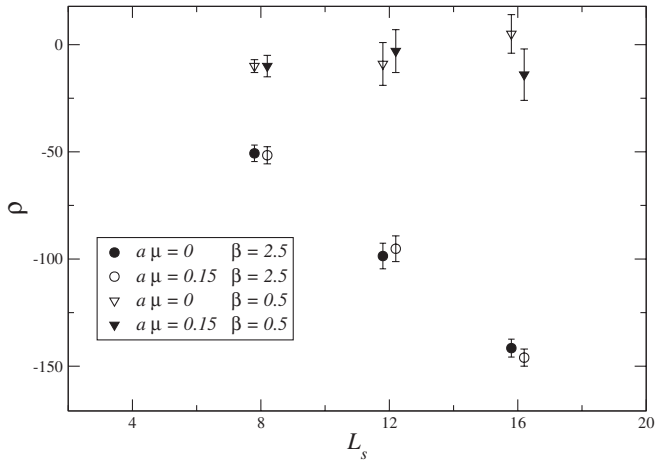

FIG. 4. Behavior of ρ in the strong coupling ($\beta = 0.5$) and in the weak coupling ($\beta = 2.5$) region as a function of L_s for $\hat{\mu} = 0$ and $\hat{\mu} = 0.15$. ρ stays constant and close to zero in the thermodynamical limit at strong coupling, while it diverges linearly with L_s at weak coupling.

assume for $\langle \mathcal{M} \rangle$ the following FSS ansatz:

$$\langle \mathcal{M} \rangle = L_s^{-(\delta/\nu)} \phi((\beta_c - \beta) L_s^{1/\nu}), \tag{19}$$

from which can be easily derived

$$\rho = L_s^{1/\nu} \tilde{\phi}((\beta_c - \beta) L_s^{1/\nu}). \tag{20}$$

We have checked this ansatz on our data, obtaining the best possible agreement for $\nu \simeq 0.63$ and $\beta_c \simeq 1.584$: a reasonable scaling is obtained, with deviations observed on the smaller lattice (see Fig. 5). In particular we estimate $\beta_c = 1.584(2)$, in good agreement with the location of the chiral transition given above. The fitted critical index ν seems to indicate an Ising 3D critical behavior, to be compared to that taking place in the quenched limit (3D Ising) and the renormalization group prediction for the critical behavior in the chiral limit (first order [44]). However, a similar finite size scaling is not observed for the other susceptibilities and we believe that a definite answer about the universality class of the transition cannot be given in the present context, also due to the relatively small spatial volume used (our largest aspect ratio is slightly less than 3). A more careful investigation should be performed and we consider the present FSS analysis, as well as that presented later for the finite density case, as only aimed at a quantitative estimate of the critical coupling where superconductivity disappears.

B. The deconfining transition at nonzero chemical potential

The two susceptibilities ρ and ρ_D permit to study $\langle \mathcal{M} \rangle$ either as a function of temperature at a fixed value of the chemical potential $\hat{\mu}$, or as a function of $\hat{\mu}$ at fixed temperature. Both strategies can be used to investigate the fate

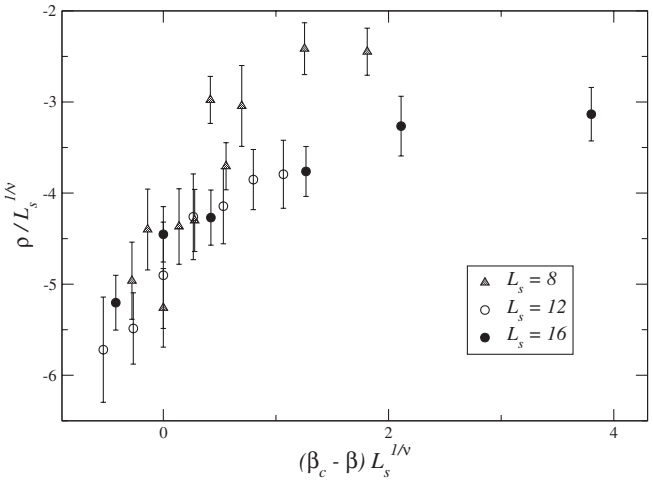

FIG. 5. Finite size scaling analysis of ρ around the transition. The best possible scaling is obtained for $\nu \simeq 0.63$ and $\beta_c \simeq 1.584$.

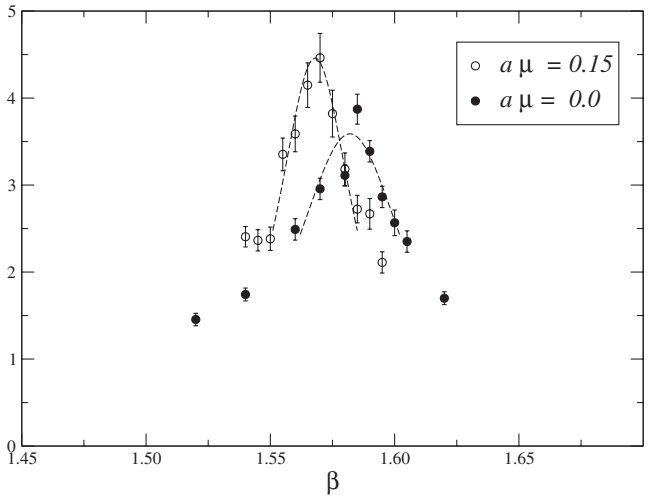

FIG. 6. Chiral susceptibility on a $16^3 \times 6$ lattice as a function of β for various values of $\hat{\mu}$. Dotted curves correspond to best fit to the peak values.

of dual superconductivity in presence of a finite density of baryonic matter: the first could be more effective at small chemical potentials, where the possible transition line starting at $\hat{\mu} = 0$ should be almost parallel to the $\hat{\mu}$ axis, the second could be more convenient at larger chemical potentials. Actually, a proper combination of ρ and ρ_D could be used to study the behavior of $\langle \mathcal{M} \rangle$ along any given path in the $\beta - \hat{\mu}$ plane, so that one could even choose an optimal combination corresponding to a relevant direction around a critical point: however we shall limit ourselves in the present context to the simpler cases of either fixed temperature or fixed chemical potential. The study at fixed temperature has a particular interest, since it may show how the disappearance of confinement (dual superconductivity) can be induced by simply increasing the density of baryonic matter.

We shall first consider the case of a fixed chemical potential, $\hat{\mu} = 0.15$. In Fig. 6 we show the chiral susceptibility obtained on a $16^3 \times 6$ lattice and compared to the same quantity computed at $\hat{\mu} = 0$. A clear shift of the pseudocritical coupling can be appreciated; in particular, we obtain $\beta_c(\hat{\mu} = 0.15) = 1.568(2)$, showing that the (pseudo)critical temperature lowers as the chemical potential is increased. Data for the susceptibility ρ on the same lattice are shown in Fig. 7 and compared to those obtained at zero density: the peak of ρ shifts consistently by an amount comparable to that of the chiral susceptibility. Notice that in both cases the actual position of the ρ peak is at a β slightly larger than β_c. That is expected since ρ is a logarithmic derivative: assuming that $\langle \mathcal{M} \rangle' \equiv \partial \langle \mathcal{M} \rangle / \partial \beta$ has a minimum at β_c (maximum slope for $\langle \mathcal{M} \rangle$), hence $\langle \mathcal{M} \rangle'' = 0$, it follows that $\partial \rho / \partial \beta = \langle \mathcal{M} \rangle'' / \langle \mathcal{M} \rangle - (\langle \mathcal{M} \rangle' / \langle \mathcal{M} \rangle)^2$ is still negative at the same point.

Data reported in Fig. 4 show that, also in the case $\hat{\mu} = 0.15$, ρ is independent of the lattice size and practically equal to zero in the strong coupling region, while it diverges linearly with L_s in the weak coupling region. Therefore we can conclude that, also in presence of a finite density of baryonic matter, dual superconductivity disappears as the temperature is increased at the same point where chiral symmetry is restored.

Next we turn to the behavior of $\langle \mathcal{M} \rangle$ as a function of $\hat{\mu}$ at fixed temperature (β), determined by means of the susceptibility ρ_D. We have considered only values of β below the (pseudo)critical coupling β_c computed at $\hat{\mu} = 0$, in particular $\beta = 1.50$ and $\beta = 1.55$: in this case we know that $\langle \mathcal{M} \rangle \neq 0$ at $\hat{\mu} = 0$, so that ρ_D may signal a possible disappearance of dual superconductivity induced by finite baryon density. Notice that the lowest value of β, on the basis of a rough two-loop estimate of the

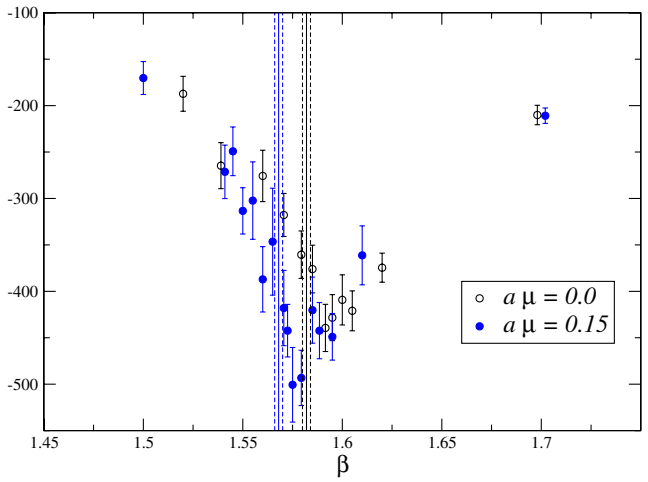

FIG. 7 (color online). ρ on a $16^3 \times 6$ lattice as a function of β for various values of $\hat{\mu}$. Vertical bands correspond to the pseudocritical value of β fitted according to the chiral susceptibility.

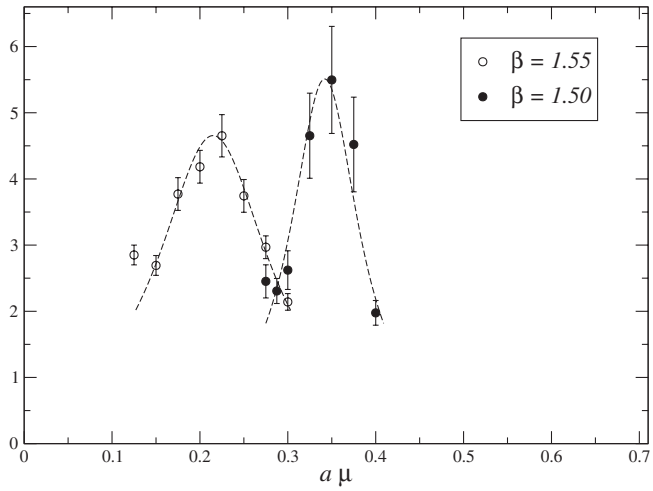

FIG. 8. Chiral susceptibility on a $16^3 \times 6$ lattice as a function of $\hat{\mu}$ for various values of β. Dotted curves correspond to best fit to the peak values.

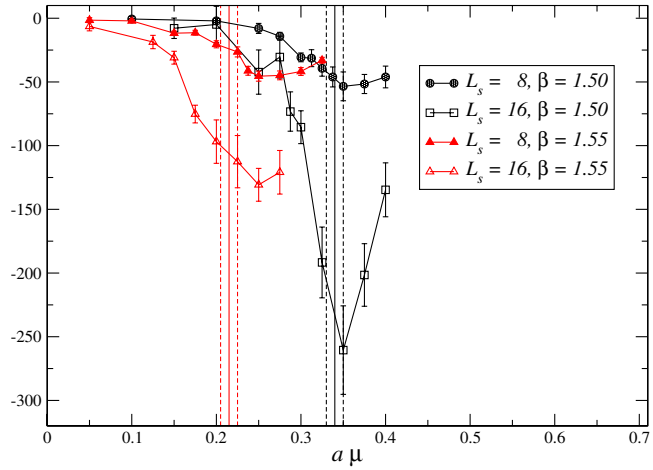

FIG. 9 (color online). ρ_D as a function of $\hat{\mu}$ and for two lattice sizes for various values of β. Vertical bands correspond to the pseudocritical chemical potential fitted according to the chiral susceptibility.

β-function, corresponds to a physical temperature $T/T_c \sim a(\beta = 1.582)/a(\beta = 1.5) \sim 0.4$, where T_c is the critical temperature at zero chemical potential.

In Fig. 8 we show the chiral susceptibility determined on a $16^3 \times 6$ lattice at $\beta = 1.55$ and $\beta = 1.50$. A best fit permits to locate the peak positions, hence the (pseudo)-critical values of $\hat{\mu}$ corresponding to chiral restoration. We obtain $\hat{\mu}_c(\beta = 1.50) = 0.340(10)$[2] and $\hat{\mu}_c(\beta = 1.55) = 0.215(10)$, as also reported in Table I.

In Fig. 9 we show instead the results obtained for ρ_D as a function of $\hat{\mu}$ at the same values of β and on various lattice sizes. It clearly appears that while ρ_D is independent of the lattice size and practically vanishing for small chemical potentials, it has a sharp negative peak in correspondence of the chiral transition which deepens as the spatial size is increased. In order to be more quantitative about the coincidence of chiral restoration and deconfinement, we have performed a FSS analysis for the case $\beta = 1.50$, where three different spatial sizes were available ($L_s = 8, 12, 16$), according to the ansatz

$$\langle \mathcal{M} \rangle = L_s^{-(\delta/\nu)} \phi((\hat{\mu}_c - \hat{\mu}) L_s^{1/\nu}), \tag{21}$$

hence

$$\rho_D = L_s^{1/\nu} \tilde{\phi}((\hat{\mu}_c - \hat{\mu}) L_s^{1/\nu}). \tag{22}$$

A reasonable scaling is obtained for $\nu \sim 0.55$ and $\hat{\mu}_c \sim 0.31$ (see Fig. 10); in particular, we estimate $\hat{\mu}_c = 0.315(15)$, marginally compatible with the location of the chiral transition.

[2]Notice that the (pseudo)critical chemical potential obtained at $\beta = 1.50$ is different from what was obtained in Ref. [4]: this difference can be understood in terms of the different algorithm used, which in the case of Ref. [4] was a nonexact molecular dynamics algorithm.

We can therefore draw two important conclusions: dual superconductivity (confinement) disappears in presence of a critical density of baryonic matter; moreover the critical line in the $T - \mu$ plane corresponding to deconfinement coincides, at least within our present uncertainties, with the chiral transition line. These results concern that part of the phase diagram including temperatures down to $T/T_c \sim 0.4$, where T_c is the critical temperature at zero chemical potential: we shall discuss their relevance for the $T \sim 0$ region of the phase diagram later in this paper.

C. The transition line

Having obtained four different locations of the transition line, in particular $\beta_c(\hat{\mu} = 0) = 1.582(2)$, $\beta_c(\hat{\mu} = 0.15) = 1.568(2)$, $\hat{\mu}_c(\beta = 1.55) = 0.215(10)$, and $\hat{\mu}_c(\beta = 1.50) = 0.340(10)$, as obtained on our larger lattices (see

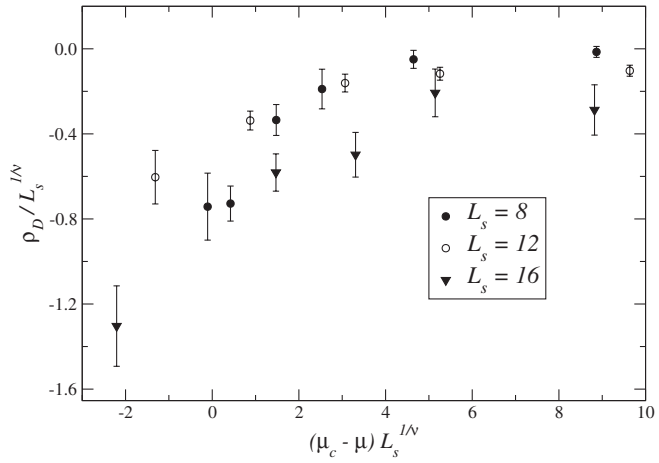

FIG. 10. Finite size scaling analysis for ρ_D. A critical index $\nu \sim 0.55$ has been used, the best value for the critical chemical potential being $\beta_c \simeq 0.315(15)$.

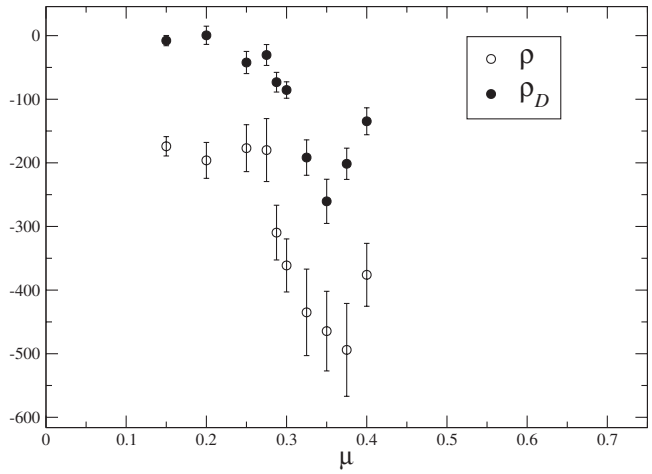

FIG. 11. Comparison of ρ and ρ_D as a function of $\hat{\mu}$ at $\beta = 1.50$ on a $16^3 \times 6$ lattice.

Table I), we can perform a fit of the dependence $\beta_c(\mu)$ in the whole $\beta - \hat{\mu}$ plane, which will then be used in the following. We are also interested in testing what was stated in Sec. III, i.e., that the ratio $-\rho_D/\rho$ at the transition point can be used as an estimate of the slope of the critical line: we give an example of a common plot of the two susceptibilities in Fig. 11, from which the ratio at β_c, $\hat{\mu}_c$ can be inferred.

We have tried a quadratic fit $\beta_c(\hat{\mu}) = A + B\hat{\mu}^2$, obtaining $A = 1.5828(16)$, $B = -0.071(4)$, and $\chi^2/\text{d.o.f.} = 0.26$. The good value of $\chi^2/\text{d.o.f.}$ shows that a quadratic dependence well describes the critical line down to $T/T_c \sim 0.5$; indeed a fit with a quartic term gives a coefficient for $\hat{\mu}^4$ compatible with zero. Our estimates for the location of the (pseudo)critical points are reported in Fig. 12 together with the fitted transition line.

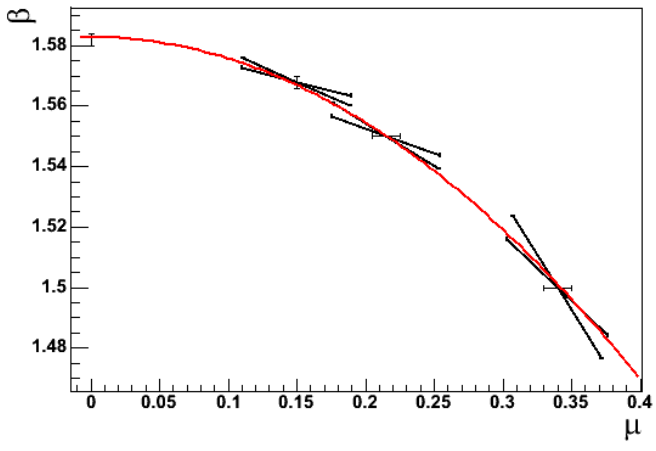

FIG. 12 (color online). Phase diagram in the $\beta - \mu$ plane. The chiral line has been fitted to a quadratic dependence on μ. The slope of the critical line, as inferred from the disorder parameter for dual superconductivity, has been reported in the figure: a nice agreement (within 1 standard deviation) can be appreciated.

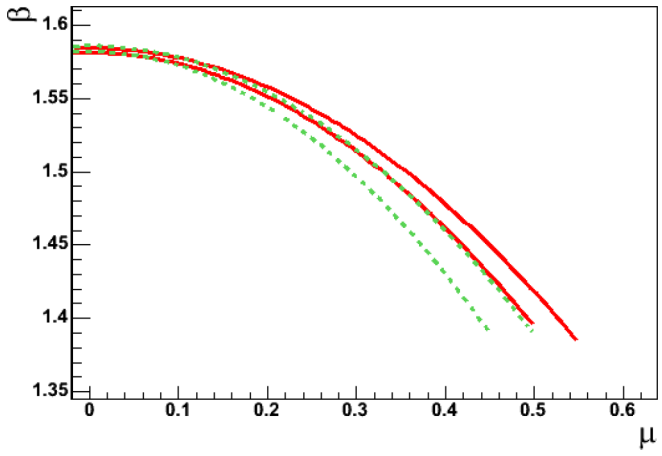

FIG. 13 (color online). Comparison of the chiral pseudocritical line (continuous) and that corresponding to the disappearance of dual superconductivity (dotted), as fitted from our data.

In correspondence of our direct locations of the transition line we also show the estimates for the slope of the line obtained from the ratio $-\rho_D/\rho$:, in particular, we have drawn angles corresponding to 1 standard deviation from the average values. A good agreement can be appreciated, showing that $-\rho_D/\rho$ can indeed be taken as a good estimator of the slope of the line in the $\beta - \hat{\mu}$ plane.

Finally, in Fig. 13, we report again the chiral transition line fitted above and compared to a quadratic fit in $\hat{\mu}$ for the critical line corresponding to the disappearance of dual superconductivity (deconfinement). The plot supports our previous statement, i.e., that the chiral transition coincides with deconfinement in the range of β values (temperatures) explored.

D. A few remarks on saturation

It is a well-known fact that, even in absence of the sign problem, the study of lattice gauge theories in the presence of a finite density of fermions cannot be pushed to arbitrarily high densities, i.e., to arbitrarily high values of the chemical potential. Indeed the number of available energy levels is limited by the presence of the UV cutoff, which places an upper limit to the possible values of the Fermi energy. Stated otherwise, we cannot place, because of the Pauli exclusion principle, more than one fermion with given quantum numbers per lattice site. Apart from the upper limit that this places on the densities reachable on the lattice, a much worse problem comes from the fact that, as saturation sets in, the absence of available fermion levels quenches fermion dynamics, modifying the field theory at the ultraviolet scale. As a matter of fact, the theory becomes equivalent to a pure gauge theory in the large $\hat{\mu}$ limit.

Saturation is therefore an unphysical lattice artifact which may in principle invalidate numerical results; one should therefore be extremely careful in locating its onset.

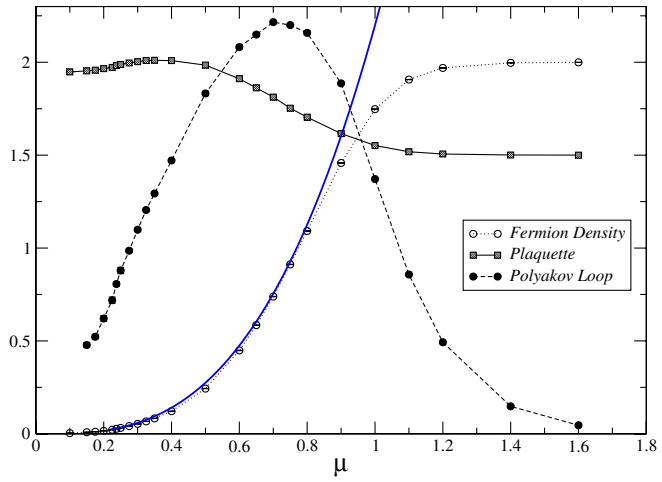

FIG. 14 (color online). Various observables computed at $\beta = 1.55$ on the $8^3 \times 6$ lattice to show saturation. The Polyakov loop has been multiplied by a factor of 8, the average plaquette by a factor of 4.

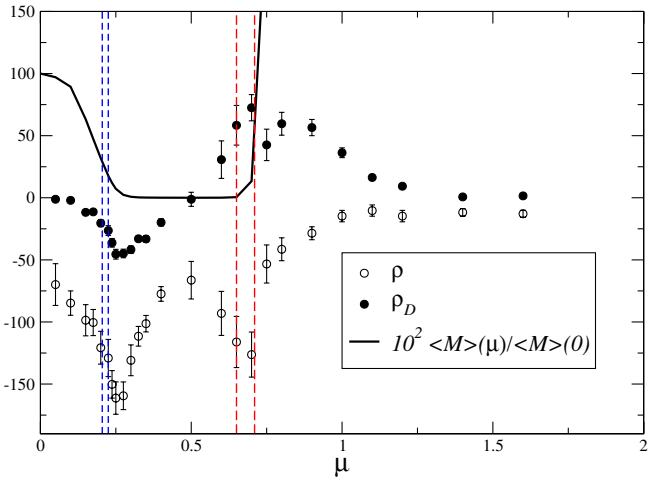

FIG. 15 (color online). ρ and ρ_D at saturation. Notice the inversion of the peaks, indicating a transition line with positive slope. Vertical dotted bands refer to the locations of the physical and saturation transition. The thick continuous line refers to the disorder parameter $\langle \mathcal{M} \rangle$ reconstructed by using the susceptibility ρ_D: after an intermediate region where the magnetic symmetry is restored, dual superconductivity sets in again in correspondence of saturation.

Indeed, while saturation effects are generically expected to appear for $\hat{\mu} = a\mu$ of order 1, the exact value of $\hat{\mu}$ where they start to be important may depend on the dynamics of the theory. In the following we will briefly explore the transition to saturation in the two-color model under consideration, arriving to some interesting conclusions which may sound as a general warning.

We have explored saturation effects in some detail at $\beta = 1.55$. In Fig. 14 we show the behavior of some observables as a function of $\hat{\mu}$ in a wide range going up to $\hat{\mu} = 1.6$. For small values of the chemical potential above $\hat{\mu}_c$ the fermion density rises roughly with a cubic dependence in $\hat{\mu}$, as expected for a gas of free fermions, but then saturates to a value which in the figure is normalized to two fermions per site: the departure from the cubic behavior starts at $\hat{\mu} \sim 0.6$–0.8. Also the rise of the Polyakov loop suddenly stops at a similar value of $\hat{\mu}$, followed by a drop; in the same region the plaquette suddenly drops towards its quenched value. Complete saturation is reached for $\hat{\mu} \sim 1.4$–1.6.

Much is learned by looking at the behavior of the susceptibilities of the disorder parameter in the same range, which is shown in Fig. 15: the negative peak of ρ_D at $\hat{\mu} \sim 0.3$, corresponding to the physical deconfinement transition, is followed by a positive unphysical peak at $\hat{\mu} \sim 0.7$. That means that the disorder parameter $\langle \mathcal{M} \rangle$, which at first drops to zero, thus signalling deconfinement, then rises again as an effect of saturation: indeed the "saturation transition" leads to an $SU(2)$ pure gauge theory, which at $\beta = 1.55$ and $L_t = 6$ is deep in the confined phase, implying $\langle \mathcal{M} \rangle \neq 0$. To verify that, we have explicitly reconstructed $\langle \mathcal{M} \rangle(\hat{\mu})/\langle \mathcal{M} \rangle(\hat{\mu} = 0)$ [see Eq. (10)] and reported it in Fig. 15: in the same figure we have reported the location of the saturation transition as obtained by a fit to the peak of the plaquette susceptibility.

We should be satisfied, since the saturation transition at $\hat{\mu} \sim 0.7$ is well separated from the physical transition at $\hat{\mu} \sim 0.3$. However we notice that, defining a "saturation line" in the $\beta - \hat{\mu}$ plane corresponding to the onset of saturation effects, we can predict, according to what stated in the previous paragraph, its slope from the ratio $-\rho_D/\rho$. We see from Fig. 15 that in correspondence of the positive saturation peak for ρ_D, the other susceptibility ρ has a negative peak, hence we expect a positive slope for the saturation line. That means that at lower values of β the onset of saturation could take place at lower values of $\hat{\mu}$: that, combined with the fact that the physical critical $\hat{\mu}_c$ instead increases as β decreases, could lead to the unfortunate situation in which the two transitions, physical and unphysical, merge at lower values of β, thus hindering, at least in the present case, the study of the strong coupling (low temperature) region of the phase diagram.

In order to further explore this possibility we have decided to make an estimate of the location of the saturation transition, through a fit to the plaquette susceptibilities (which are reported in Fig. 16), performing simulations also at a different value of the gauge coupling, $\beta = 1.675$. Our estimates for the pseudocritical saturation chemical potential μ_{Sc} are reported in Table I and are $\hat{\mu}_{Sc}(\beta = 1.55) = 0.68(3)$ and $\hat{\mu}_{Sc}(\beta = 1.675) = 0.79(3)$. In Fig. 17 we report our estimate for the location of the saturation line together with a rough linear extrapolation suggesting that this line could meet the physical transition line, whose estimate given in previous paragraph is reported in the figure as well, for $\beta \sim 1.4$. Notice that the linear extrapolation adopted is supported by the slope of

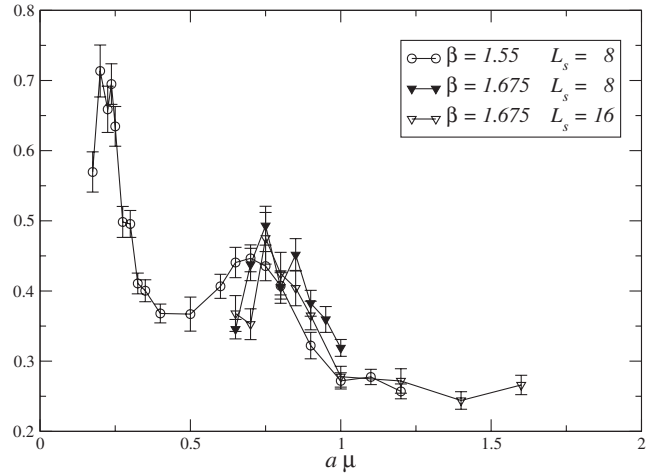

FIG. 16. Plaquette susceptibilities used to locate the saturation transition.

the line obtained through the ratio $-\rho_D/\rho$, whose estimates are reported in the figure as well.

We therefore give a general warning about the possible effects of saturation on the study of finite density QCD at low values of the gauge coupling. The situation may of course be quite different depending on the temporal extent L_t of the lattice, on the number of flavors, of colors, and on the lattice discretization (staggered or Wilson fermions) adopted. In particular, increasing L_t one should approach the continuum limit, hence the physical transition line should move to smaller values of $\hat{\mu} = a\mu$, thus becoming more separated from the unphysical saturation line. The problem should be milder with Wilson fermions; indeed in this case saturation is known to set in at larger values of $\hat{\mu}$ [2,45]. Improved lattice actions may also be of great benefit [45]. We plan to make a more extensive study of this problem in the future.

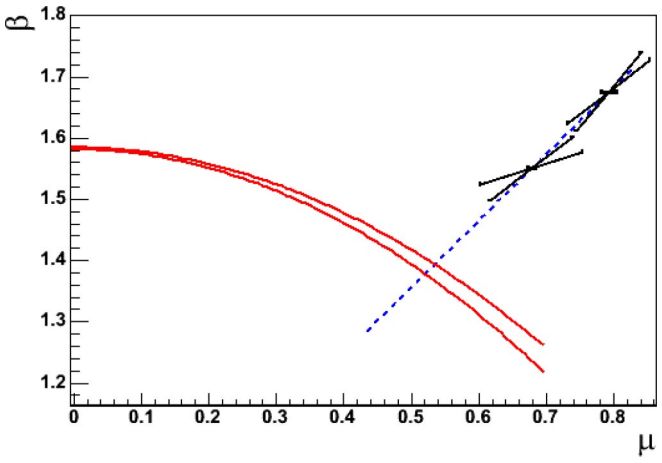

FIG. 17 (color online). Saturation transition line and its relation with the physical transition line.

E. Did we catch the physics of the low temperature region of the phase diagram?

One of our starting questions was about the fate of confinement at high densities and low temperatures, since that could help in understanding the nature of compact astrophysical objects. In Ref. [2] the hypothesis has been made, based on the analysis of the Polyakov loop, that at $T \sim 0$ deconfinement could occur at a critical density following and well separated from the onset of a bosonic superfluid phase. It is natural to ask whether our present results can be of any relevance regarding this specific issue, i.e., how close we have got to the low temperature region of the QCD phase diagram.

Since we have not included an explicit diquark source term in our model, we cannot obtain direct information about that observable; however we shall try to sketch a qualitative picture based on the distribution of the eigenvalues of the fermionic matrix. At zero density that can be written as $M = am\mathrm{Id} + D$ where D is anti-Hermitian, hence it has purely imaginary eigenvalues, therefore the eigenvalues of M lie on a segment in the complex plane orthogonal to the real axis.

As a real chemical potential is switched on, D ceases to be anti-Hermitian and the eigenvalues get scattered in the whole complex plane: that is evident in the first part of Fig. 18, where we show the distribution of eigenvalues on a typical configuration obtained at $\beta = 1.55$ and a small chemical potential, $\hat{\mu} = 0.10$. The eigenvalues occupy a narrow vertical band and the finite density of eigenvalues in correspondence of the real axis is strictly linked to the presence of chiral symmetry breaking (Banks-Casher relation [46]) The width of the distribution on the real axis grows as $\hat{\mu}$ increases, roughly proportionally to $\hat{\mu}^2$, till the distribution touches the imaginary axis: at this point the chiral condensate is expected to rotate into a diquark condensate (see, for instance, Ref. [47] for a review): as it is clear from the second part of Fig. 18, at $\beta = 1.55$ this happens roughly at $\hat{\mu} \sim 0.3$, a value which actually turns out to be almost independent of the gauge coupling in the range of β values explored in our simulations and is in agreement with the values found for diquark condensation in similar works using the same quark mass [34,48]: we show as an example in Fig. 19 the eigenvalue distribution, as obtained on typical configurations, projected onto the real axis for three values of $\hat{\mu}$ at $\beta = 1.45$.

However, if we are in the high temperature region, i.e., slightly below $T_c(\mu = 0)$, chiral symmetry will be restored quite soon as $\hat{\mu}$ is increased because of the transition to the quark-gluon plasma. Therefore there will be actually no chiral condensate to be rotated into a diquark condensate at the point where the distribution touches the imaginary axis. Indeed we see from the second part of Fig. 18 that the region around the real axis is quite depleted of eigenvalues for $\beta = 1.55$ at $\hat{\mu} = 0.3$. We can easily understand this in terms of the chiral line we have drawn in Fig. 12:

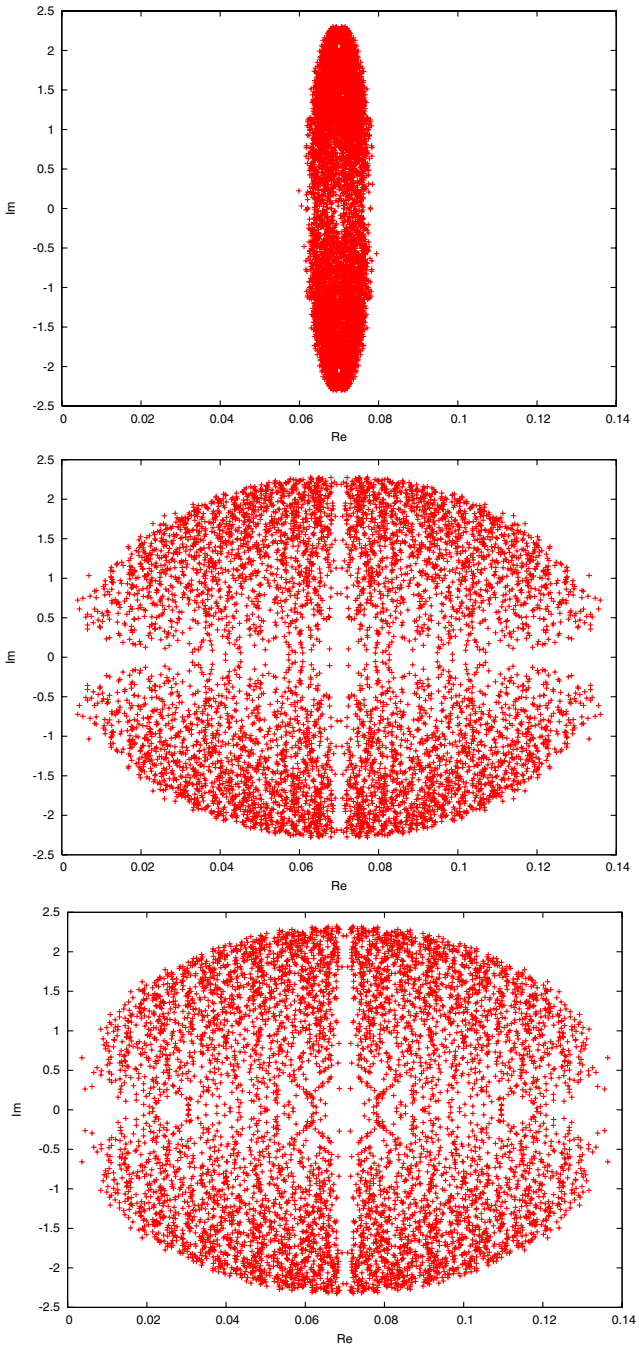

FIG. 18 (color online). Distribution of eigenvalues on typical configurations of the $8^3 \times 6$ lattice obtained, respectively, at ($\beta = 1.55$, $\hat{\mu} = 0.10$), ($\beta = 1.55$, $\hat{\mu} = 0.30$), and ($\beta = 1.45$, $\hat{\mu} = 0.30$).

chiral symmetry gets restored already below $\hat{\mu} = 0.3$ at $\beta = 1.55$.

Following this line of reasoning, the region relevant for low temperature physics on our lattices with $L_t = 6$ should be that below $\beta \sim 1.5$, where our fitted (pseudo)critical line passes beyond $\hat{\mu} \sim 0.3$. In this region one could for instance observe, among other different possibilities, two

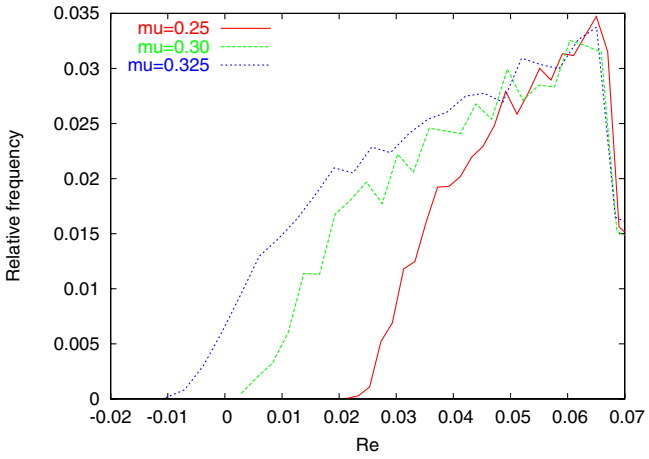

FIG. 19 (color online). Distribution of eigenvalues projected onto the real axis for various $\hat{\mu}$ on a $8^3 \times 6$ lattice at $\beta = 1.45$.

different transitions, the first corresponding to the onset of diquark condensation, the second roughly being the continuation of the line in Fig. 12, thus corresponding to deconfinement: this is indeed the scenario suggested by Ref. [2].

We have therefore performed numerical simulations on a $8^3 \times 6$ lattice at $\beta = 1.45$. In this case a finite density of eigenvalues around the real axis is still present at $\hat{\mu} \sim 0.3$, as can be better appreciated from Fig. 20, where we plot the distribution projected onto the imaginary axis at $\beta = 1.45$ and $\hat{\mu} = 0.3$, compared to that obtained at higher temperatures.

In Fig. 21 we report the chiral susceptibility compared to that measured on the same lattices at different gauge couplings. We notice that the peak is strongly reduced and its position is not much different from what was obtained at $\beta = 1.5$ and in clear disagreement with what was expected from the continuation of the chiral line in

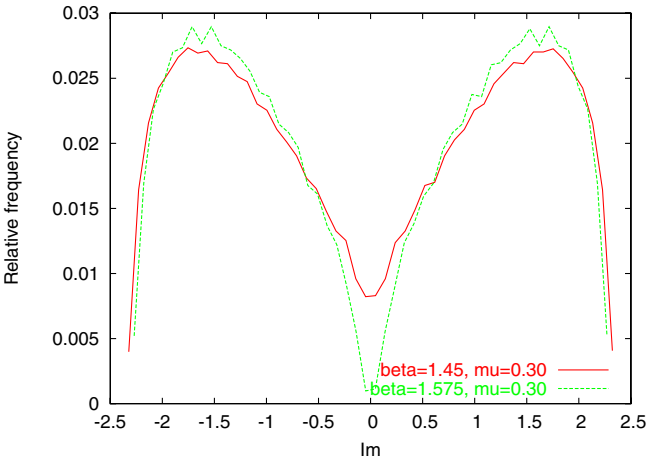

FIG. 20 (color online). Distribution of eigenvalues projected onto the imaginary axis for various values of β on a $8^3 \times 6$ lattice at $\hat{\mu} = 0.3$.

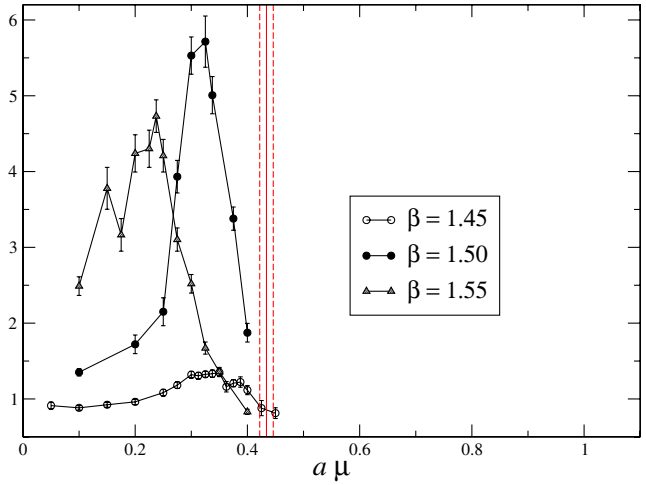

FIG. 21 (color online). Chiral susceptibilities on the $8^3 \times 6$ lattice at various values of β.

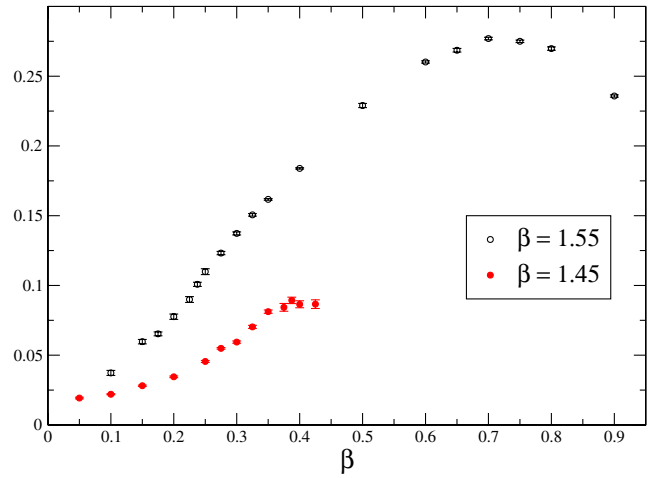

FIG. 23 (color online). Polyakov loop at various values of β on a $8^3 \times 6$ lattice.

Fig. 12. The first peak could indeed correspond to the onset of a bosonic superfluid phase. Nothing seems to happen thereafter.

In Fig. 22 we report instead data obtained for the susceptibility ρ_D of the disorder parameter. In this case the negative peak has almost completely disappeared and a very small peak at $\hat{\mu} \sim 0.3$ is followed by a region $\hat{\mu} \geq 0.4$ where ρ_D clearly changes its sign: on the basis of what we have discussed in Sec. IV D and comparing this behavior with that observed at $\beta = 1.55$, a possible interpretation is that of an early onset of saturation effects in this case, preventing the observation of any further physical transition. We expected saturation effects to obscure the physical transition at $\beta \sim 1.4$, but we are not surprised that the situation may be worse.

This conclusion is supported by looking at the behavior of the Polyakov loop (see Fig. 23), in this case saturation

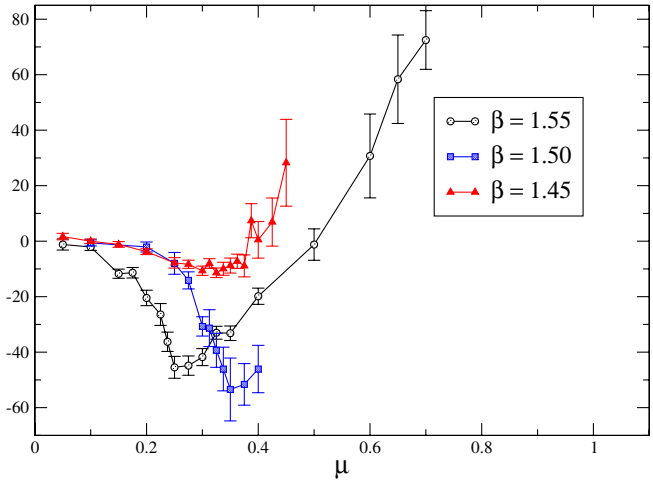

FIG. 22 (color online). ρ_D at various values of β on a $8^3 \times 6$ lattice.

effects are signaled by an inversion in the growth of $\langle L \rangle$ as a function of $\hat{\mu}$.

We conclude therefore that we are not able to clarify the onset of deconfinement at $T \sim 0$, at least on the present lattice size. We could of course further decrease the temperature without decreasing β by going to larger values of L_t. However that would imply a numerical effort which is not affordable with our present algorithmic and computational resources.

V. CONCLUSIONS

We have investigated the phase diagram of two-color QCD at finite temperature and density by means of a disorder parameter for color confinement detecting dual superconductivity of the QCD vacuum.

We have obtained evidence for deconfinement induced by a finite density of baryonic matter. Moreover the transition line corresponding to the disappearance of dual superconductivity (deconfinement) appears to coincide, in the range of temperature explored ($0.4T_c < T < T_c$, where T_c is the critical temperature at zero density), with that corresponding to chiral symmetry restoration, as it happens in the zero density case. We think that this result could be relevant also for three-color QCD, at least in the range of relatively high temperatures explored in this paper, where the differences between $N_c = 2$ and $N_c = 3$ should be less important also in the case of chiral properties. We have also shown that the susceptibilities of the disorder parameter can be used in order to compute the slope of the critical line in the $\beta - \hat{\mu}$ plane, obtaining consistent results.

We have investigated in some detail the unphysical transition corresponding to the onset of saturation and shown that it moves at lower values of $\hat{\mu}$ as β is decreased with a possible intersection with the physical transition line, thus giving a general warning about the possible

effects of saturation on the study of finite density QCD at strong values of the gauge coupling. As discussed at the end of Sec. IV D, this phenomenon of course may be quite different depending on the fermion discretization (staggered or Wilson, standard or improved lattice action), on the number of flavors and on other parameters of the system (L_t, quark masses); for this reason we plan to make a more systematic study in the future. We have also verified that in our case saturation actually prevents us from obtaining results relevant for the $T \sim 0$ region of the phase diagram.

Let us discuss possible future improvements of our present investigation. The use of larger values of L_t will be an important point: it will permit us to study the approach to the continuum limit of our results and, by better separating the physical transition from the saturation region, it will let us explore lower temperatures. In the present study we have used staggered fermions corresponding to $N_f = 8$ continuum flavors, the reason being that an exact hybrid Monte Carlo algorithm is available in this case and no root trick is needed to reduce the number of flavors; the same theory has indeed been investigated by other groups in the past. However, the dependence on the number of flavors may be important, especially in the theory with two colors, where different nontrivial fixed points may appear for large N_f. Therefore a comparison with results obtained at different values of N_f will surely be useful.

Finally, results relevant for the high temperature region of real QCD could also be obtained by studying QCD at finite isospin density or within the imaginary chemical potential approach.

ACKNOWLEDGMENTS

We thank Ph. de Forcrand, A. Di Giacomo, M. P. Lombardo, B. Lucini, and E. Vicari for useful discussions. Numerical simulations have been run on a PC farm at INFN-Genova and on the INFN apeNEXT facility in Rome. Simulations on the smaller lattices have been performed by means of a numerical code obtained by adapting the publicly available MILC Collaboration code.

[1] L. McLerran and R. D. Pisarski, arXiv:0706.2191.
[2] S. Hands, S. Kim, and J. I. Skullerud, Eur. Phys. J. C **48**, 193 (2006).
[3] M. D'Elia and M. P. Lombardo, Phys. Rev. D **67**, 014505 (2003); **70**, 074509 (2004).
[4] B. Alles, M. D'Elia, and M. P. Lombardo, Nucl. Phys. **B752**, 124 (2006).
[5] G. 't Hooft, in *High Energy Physics, Proceedings of the EPS International Conference, Palermo, 1975*, edited by A. Zichichi, (Editrice Compositori, Bologna, 1976).
[6] S. Mandelstam, Phys. Rep. **23**, 245 (1976).
[7] G. Parisi, Phys. Lett. **60B**, 93 (1975).
[8] L. Del Debbio, A. Di Giacomo, and G. Paffuti, Phys. Lett. B **349**, 513 (1995).
[9] A. Di Giacomo and G. Paffuti, Phys. Rev. D **56**, 6816 (1997).
[10] A. Di Giacomo, B. Lucini, L. Montesi, and G. Paffuti, Phys. Rev. D **61**, 034503 (2000); **61**, 034504 (2000).
[11] J. M. Carmona, M. D'Elia, A. Di Giacomo, B. Lucini, and G. Paffuti, Phys. Rev. D **64**, 114507 (2001).
[12] J. M. Carmona, M. D'Elia, L. Del Debbio, A. Di Giacomo, B. Lucini, and G. Paffuti, Phys. Rev. D **66**, 011503 (2002).
[13] M. D'Elia, A. Di Giacomo, B. Lucini, C. Pica, and G. Paffuti, Phys. Rev. D **71**, 114502 (2005).
[14] M. N. Chernodub, M. I. Polikarpov, and A. I. Veselov, Phys. Lett. B **399**, 267 (1997).
[15] P. Cea and L. Cosmai, J. High Energy Phys. 11 (2001) 064; P. Cea, L. Cosmai, and M. D'Elia, J. High Energy Phys. 02 (2004) 018.
[16] J. Frohlich and P. A. Marchetti, Phys. Rev. D **64**, 014505 (2001).
[17] M. D'Elia, S. Conradi, and A. D'Alessandro, Proc. Sci., LAT2006 (2006) 131.
[18] Z. Fodor and S. D. Katz, Phys. Lett. B **534**, 87 (2002); J. High Energy Phys. 03 (2002) 014.
[19] Z. Fodor, S. D. Katz, and C. Schmidt, J. High Energy Phys. 03 (2007) 121.
[20] Ph. de Forcrand and O. Philipsen, Nucl. Phys. **B642**, 290 (2002); **B673**, 170 (2003).
[21] V. Azcoiti, G. Di Carlo, A. Galante, and V. Laliena, Nucl. Phys. **B723**, 77 (2005).
[22] H. S. Chen and X. Q. Luo, Phys. Rev. D **72**, 034504 (2005).
[23] P. Giudice and A. Papa, Phys. Rev. D **69**, 094509 (2004)
[24] P. Cea, L. Cosmai, M. D'Elia, and A. Papa, J. High Energy Phys. 02 (2007) 066.
[25] M. D'Elia, F. Di Renzo, and M. P. Lombardo, arXiv:0705.3814.
[26] A. Roberge and N. Weiss, Nucl. Phys. **B275**, 734 (1986).
[27] S. Kratochvila and P. de Forcrand, Proc. Sci., LAT2005 (2006) 167.
[28] A. Alexandru, M. Faber, I. Horvath, and K. F. Liu, Phys. Rev. D **72**, 114513 (2005).
[29] C. R. Allton *et al.*, Phys. Rev. D **66**, 074507 (2002); **71**, 054508 (2005).
[30] R. V. Gavai and S. Gupta, Phys. Rev. D **68**, 034506 (2003); **73**, 014004 (2006).
[31] T. C. Blum, J. E. Hetrick, and D. Toussaint, Phys. Rev. Lett. **76**, 1019 (1996).
[32] J. Engels, O. Kaczmarek, F. Karsch, and E. Laermann, Nucl. Phys. **B558**, 307 (1999).

[33] R. De Pietri, A. Feo, E. Seiler, and I. O. Stamatescu, arXiv:0705.3420.
[34] S. Hands, J. B. Kogut, M. P. Lombardo, and S. E. Morrison, Nucl. Phys. **B558**, 327 (1999).
[35] R. Aloisio, V. Azcoiti, G. Di Carlo, A. Galante, and A. F. Grillo, Phys. Lett. B **493**, 189 (2000).
[36] S. Hands, I. Montvay, L. Scorzato, and J. Skullerud, Eur. Phys. J. C **22**, 451 (2001).
[37] J. B. Kogut, D. K. Sinclair, S. J. Hands, and S. E. Morrison, Phys. Rev. D **64**, 094505 (2001).
[38] J. B. Kogut, D. Toublan, and D. K. Sinclair, Nucl. Phys. **B642**, 181 (2002).
[39] S. Muroya, A. Nakamura, and C. Nonaka, Phys. Lett. B **551**, 305 (2003).
[40] S. Chandrasekharan and F. J. Jiang, Phys. Rev. D **74**, 014506 (2006).
[41] M. D'Elia and L. Tagliacozzo, Phys. Rev. D **74**, 114510 (2006).
[42] S. A. Gottlieb, W. Liu, D. Toussaint, R. L. Renken, and R. L. Sugar, Phys. Rev. D **35**, 2531 (1987).
[43] M. D'Elia, A. Di Giacomo, and B. Lucini, Phys. Rev. D **69**, 077504 (2004).
[44] J. Wirstam, Phys. Rev. D **62**, 045012 (2000).
[45] W. Bietenholz and U. J. Wiese, Phys. Lett. B **426**, 114 (1998).
[46] T. Banks and A. Casher, Nucl. Phys. **B169**, 103 (1980).
[47] K. Splittorff and J. J. M. Verbaarschot, arXiv:0704.0330.
[48] E. Bittner, M. P. Lombardo, H. Markum, and R. Pullirsch, Nucl. Phys. B, Proc. Suppl. **94**, 445 (2001).